Field-induced orbital distortion in high-order-harmonic generation from aligned and oriented molecules within adiabatic strong-field approximation

Maciej Dominik Śpiewanowski and Lars Bojer Madsen
Department of Physics and Astronomy, Aarhus University, DK-8000 Aarhus C, Denmark
(Received 3 July 2013; revised manuscript received 22 November 2013; published 10 April 2014)

We describe high-order-harmonic generation (HHG) within the adiabatic strong-field approximation (ASFA) where the ground state and its energy adiabatically follows the instantaneous external field and within the Stark-shift-corrected SFA (SSFA), where only the energy shift is accounted for. We show that the molecular polarizability reflects the significance of field-induced orbital distortion in the HHG process. We show that for CO_2, which possesses a relatively low polarizability, the two-center interference minimum can be clearly seen in both the ASFA and the SSFA. This finding is in agreement with experimental data at large wavelength. Moreover, we introduce a method for analyzing the recombination events. This method relies on averaging the recombination matrix elements weighted with the photon emission probability of each harmonic. In the case of CO_2 this method confirms that the interference minimum is determined by recombination to the two O atoms. We use the example of N_2O, which has a moderate polarizability, to show that the number of centers taking part in the creation of the interference minimum may change depending on the intensity. Finally, we show that in the short-pulse limit, the minimum in the HHG spectrum from oriented N_2O strongly depends on the molecular orientation and carrier-envelope phase.

DOI: 10.1103/PhysRevA.89.043407 PACS number(s): 33.20.Xx, 42.50.Hz, 42.65.Ky

I. INTRODUCTION

When an intense laser pulse interacts with an atomic or molecular target radiation of harmonics up to very high orders of the fundamental frequency of the driving laser light can be generated [1]. Apart from the interest in high-order-harmonic generation (HHG) as a source of coherent short-wavelength light with unique properties, the interest is fueled by the unique information on specific atoms and molecules carried by HHG spectra. For example, the information encoded in the spectrum allows an elucidation of internuclear separations [2–5] and molecular orbitals [6–10]. The physics of HHG is captured by the three-step model [11,12]. First, a bound electron is driven into the continuum via tunneling ionization. Second, the continuum electron acquires energy by its acceleration in the field. Third, the electron recombines into the original bound state, emitting the excess energy as radiation.

One of the characteristic features of molecular HHG spectra is the presence of a minimum. The minimum may have different origin depending on the target molecule and laser parameters. Therefore, different information about the molecule may be extracted from its position and its behavior with respect to changing field parameters and molecular alignment and orientation. For example, the interplay between the highest occupied molecular orbital (HOMO) and lower-lying orbitals in the HHG process [13–15] can be elucidated by studying the dynamic minimum created by destructive interference of signals from multiple orbitals. Information about the electronic structure of the target can be deduced from the presence of a Cooper minimum [16–20]. Finally, an interference between the radiation emitted from different centers gives rise to what is referred to as a two-center interference minimum, although more centers may participate. This is the type of minima of concern in this work and these minima allow the extraction of structural information about the target [21–24].

One of the models that keeps the simple physical picture of the three-step model and qualitatively describes many HHG phenomena is the strong-field approximation (SFA) for HHG, also sometimes referred to as the Lewenstein model [25]. In the SFA, the full evolution operator is replaced by the Volkov evolution operator and the full scattering state is replaced by the momentum eigenstate [26,27]. In this approach the influence of the field on initial and final bound-state orbitals is neglected and therefore phenomena such as the Stark shift of the energy levels and field-induced orbital distortion are not accounted for. An extension of the SFA for HHG to include Stark shifting of the energy levels for polar molecules was presented in Ref. [28]. We refer to this approximation as the Stark-shift-corrected SFA (SSFA). The SSFA has been applied to the study of HHG from polar molecules in a number of papers [29–34]. Very recently the model of Ref. [28] was extended to take into account the effect of field distortion of the bound-state orbitals [35], an approach that we refer to as the adiabatic SFA (ASFA). The effects of field distortion of molecular orbitals on the HHG spectrum were studied for model molecules with the use of the multiconfiguration time-dependent Hartree (MCTDH) method in Ref. [36]. For the case of a one-dimensional zero-range potential, the adiabatic theory for HHG, without the additional SFA simplifications, was presented in Ref. [37].

The ASFA [35] showed, using the example of N_2, that the observation of a two-center interference minimum may be hindered by field distortion of the molecular orbitals taking part in the process, which is in agreement with MCTDH calculations [36]. Hence, using the ASFA, it was possible to suggest the reason why so far no experimental data [6,38,39] have revealed a two-center interference minimum in HHG spectra of N_2. On the other hand, experimental data show a clear two-center interference minimum for a variety of molecular species including CO_2. For the case of CO_2 the experimental results [10] show a clear two-center interference

minimum for field strengths far exceeding the one used in Ref. [35] for N_2. This indicates that the field-induced orbital distortion does not influence the HHG spectra for CO_2. These findings, viz., the lack of the two-center interference minimum in HHG spectra from N_2 and the presence of a clear minimum in HHG spectra from CO_2, hint at the existence of a third group of molecules, namely, molecules for which the field-induced orbital distortion is moderate. For such molecules one may expect that the depth and the position of the minimum change with the laser intensity. Such a change in the spectrum was up to now thought to be a typical feature of a so-called dynamic minimum [13–15,40]. The influence of the field distortion on the HHG process requires further investigation and this is the topic of this paper.

In this paper we discuss the ASFA. It was used in Ref. [35] without a detailed discussion of the approximation. In the standard SFA the active bound-state orbital participating in the ionization and recombination steps is taken as a field-free orbital. In the ASFA this active orbital is taken as an adiabatic eigenstate of the instantaneous Hamiltonian. This adiabatic approximation is justified in the long-wavelength limit since the electromagnetic field then changes on much slower time scales than the time scale associated with the electronic bound-state motion; in other words, in this limit the ionization potential I_p is much larger than the photon energy ω_L (atomic units are used throughout unless indicated otherwise). We apply the ASFA and the SSFA to HHG calculations for CO_2. The HOMO of this molecule has a relatively low polarizability, therefore the distortion due to the driving laser field is insignificant. The calculated HHG spectra in both the ASFA and the SSFA agree very well with experimental data [10]. In particular, the minimum does not disappear with increasing intensity. In the analysis of the origin of the interference minimum, we introduce a method to study the recombination events during the whole HHG process and use it to confirm the negligible influence of the field distortion in the case of CO_2. By the example of N_2O we study a case with an intermediate polarizability. This choice enables us to observe the changing influence of the field distortion with changing field strength and a difference in the ASFA and SSFA predictions. Finally we show that for very short pulses the minimum in the HHG spectrum from oriented N_2O strongly depends, due to its permanent dipole moment and polarizability, on the orientation of the molecule with respect to the polarization of the driving field as well as on the carrier-envelope phase.

The paper is organized as follows. In Sec. II we recall the basis formulas for modeling of the HHG signal from a single molecule. Then in Sec. II A we consider the standard SFA. We include this discussion for completeness and to be able to highlight the approximations and compare them with the approximations entering the formulation of the ASFA presented in Sec. II B. Section III presents the results. In Sec. III A we discuss the predictions for CO_2 and introduce the analysis in terms of averaged recombinations matrix elements. In Sec. III B we turn to N_2O and discuss the influence of the dipole and the sensitivity of the HHG spectra to the field parameters as a consequence of orbital distortion. In Sec. III C we present the results of a study on HHG from N_2O from a two-cycle pulse. Section IV summarizes.

II. THEORY

The HHG spectrum $S_{\boldsymbol{n}}(\omega)$ of the harmonic component along $\boldsymbol{n}$ is taken to be [41]

$$S_{\boldsymbol{n}}(\omega) = \left| \int_{-\infty}^{\infty} \boldsymbol{n} \cdot \langle \boldsymbol{v}(t) \rangle e^{i\omega t} dt \right|^2, \tag{1}$$

where $\langle \boldsymbol{v}(t) \rangle$ is the expectation value of the dipole velocity operator. Let the z axis be parallel to the linear polarization of the driving laser field. The orientation of the molecule with respect to this axis is specified by the three Euler angles $\mathcal{R} = (\alpha, \beta, \gamma)$, where α denotes the angle of rotation around the z axis, β denotes the angle of rotation around the new y axis, and γ denotes the angle of rotation around the molecular axis. The orientational distribution $\mathcal{G}(\mathcal{R})$ of the molecule is factored out as a coherent sum [42,43]

$$\langle \boldsymbol{v}(t) \rangle = \int \mathcal{G}(\mathcal{R}) \langle \boldsymbol{v}(\mathcal{R}, t) \rangle d\mathcal{R}. \tag{2}$$

For a given fixed orientation $\mathcal{R}$, the state $|\Psi(t)\rangle$ needed for the evaluation of the expectation value of the dipole velocity solves the time-dependent Schrödinger equation

$$i\,\partial_t |\Psi(t)\rangle = H(t) |\Psi(t)\rangle, \tag{3}$$

with

$$H(t) = H_0 + \sum_i \boldsymbol{F}(t) \cdot \boldsymbol{r}_i, \tag{4}$$

where H_0 is the field-free Hamiltonian and $\boldsymbol{F}(t)$ is an infrared or near-infrared electromagnetic field, which is turned on at time $t = 0$ and off at time $t = T$. For notational convenience, we suppress the dependence on $\mathcal{R}$ in the specification of the quantum states. The exact numerical solution of Eq. (3) is impossible for polyatomic, multielectron molecules at the wavelengths and field strengths of interest. Approximations are therefore needed. In the next section we summarize the evaluation of $|\Psi(t)\rangle$ and $\langle \boldsymbol{v}(\mathcal{R}, t) \rangle$ within the SFA [25]. This discussion serves as background for the formulation of the ASFA following in Sec. II B.

A. State $|\Psi(t)\rangle$ and dipole velocity expectation value within the SFA

Within the SFA, the state $|\Psi(t)\rangle$ is approximated in the following way. First the problem is reduced to the consideration of a single active orbital $|\psi(t)\rangle$. This simplification may be realized by freezing all but the active orbital, which we denote as the HOMO in the following. The evolution of the HOMO is then represented by the essential state expansion

$$|\psi(t)\rangle = c_0(t) |\phi_0\rangle e^{-i E_0 t} + \int c_{\boldsymbol{k}}(t) |\boldsymbol{k}(t)\rangle \exp\left(-i \int_0^t E_{\boldsymbol{k}}(t') dt' \right) d\boldsymbol{k}, \tag{5}$$

where $|\phi_0\rangle$ is the HOMO with binding energy E_0, solving the equation

$$f_0 |\phi_0\rangle = E_0 |\phi_0\rangle, \tag{6}$$

with the field-free Fock operator given in terms of the kinetic energy and the Hartree-Fock (HF) potential

$$f_0 = \frac{p^2}{2} + V^{\mathrm{HF}}. \tag{7}$$

In Eq. (5) the state

$$|\boldsymbol{k}(t)\rangle = |\boldsymbol{k} + \boldsymbol{A}(t)\rangle \tag{8}$$

is a momentum eigenstate with position representation

$$\langle \boldsymbol{r}|\boldsymbol{k}(t)\rangle = \frac{1}{(2\pi)^{3/2}} e^{i\boldsymbol{k}(t)\cdot\boldsymbol{r}} \tag{9}$$

such that $|\boldsymbol{k}(t)\rangle \exp[-i\int_0^t E_{\boldsymbol{k}}(t')dt']$ is the Volkov state with energy

$$E_{\boldsymbol{k}}(t) = k(t)^2/2 = [\boldsymbol{k} + \boldsymbol{A}(t)]^2/2, \tag{10}$$

which solves the Schrödinger equation for a free electron in the presence of the electromagnetic field and where $\boldsymbol{A}(t)$ denotes the momentum gained by the electron from the electric field

$$\boldsymbol{A}(t) = -\int_0^t \boldsymbol{F}(t')dt'. \tag{11}$$

In Eq. (5) the time-dependent $c_0(t)$ and $c_{\boldsymbol{k}}(t)$ coefficients are unknown. To determine them, we insert Eq. (5) into

$$i\,\partial_t|\psi(t)\rangle = [f_0 + \boldsymbol{F}(t)\cdot\boldsymbol{r}]|\psi(t)\rangle \tag{12}$$

and project on $\langle\boldsymbol{k}(t)|$ and $\langle\phi_0|$. This leads to a set of first-order linear differential equations for the expansion coefficients. To simplify these equations (see Ref. [25]) (i) depletion of the ground state is neglected, i.e., $c_0(t) \approx 1$, (ii) the overlap $\langle\boldsymbol{k}(t)|\phi_0\rangle$ is neglected, (iii) the laser-induced continuum-continuum couplings are neglected, i.e., $\langle\boldsymbol{k}(t)|\boldsymbol{F}(t)\cdot\boldsymbol{r}|\boldsymbol{k}'(t)\rangle \approx 0$, and (iv) the terms $\langle\boldsymbol{k}(t)|V^{\mathrm{HF}}|\boldsymbol{k}'(t)\rangle$ are neglected. The equation for the amplitude in the continuum then fulfils the differential equation

$$\dot{c}_{\boldsymbol{k}}(t) = -i\langle\boldsymbol{k}(t)|\boldsymbol{F}(t)\cdot\boldsymbol{r}|\phi_0\rangle \exp\left(i\int_0^t (E_{\boldsymbol{k}}(t') - E_0)dt'\right), \tag{13}$$

which is recognized as the standard expression from time-dependent first-order perturbation theory for a transition from $|\phi_0\rangle$ induced by the external field to the Volkov state. Equation (13) is readily integrated and the result for the active orbital in the SFA reads

$$|\psi(t)\rangle = |\phi_0\rangle e^{-iE_0t} - i\int\int_0^t |\boldsymbol{k}(t)\rangle\langle\boldsymbol{k}(t')|\boldsymbol{F}(t')\cdot\boldsymbol{r}|\phi_0\rangle \times \exp\left(-i\int_{t'}^t E_{\boldsymbol{k}}(t'')dt'' - i\int_0^{t'} E_0 dt''\right)dt'd\boldsymbol{k}. \tag{14}$$

The first term on the right-hand side (rhs) of Eq. (14) describes evolution in the ground state. The second term describes evolution in the ground state from time $t = 0$ and then evolution in the Volkov continuum from the ionization time t' to the instant of interest t. The SFA ionization matrix element is readily identified in the last term. The state $|\psi(t)\rangle$ can now be inserted into Eq. (2) and the standard SFA expression for the expectation value of the dipole is regained

$$\langle\boldsymbol{v}(\mathcal{R},t)\rangle = -i\int\int_0^t \boldsymbol{M}_{\mathrm{rec}}(\mathcal{R},\boldsymbol{k},t) \times \exp\left(-i\int_{t'}^t (E_{\boldsymbol{k}}(t'') - E_0)dt''\right) \times M_{\mathrm{ion}}(\mathcal{R},\boldsymbol{k},t')dt'd\boldsymbol{k} + \mathrm{c.c.}, \tag{15}$$

with ionization at time t'

$$M_{\mathrm{ion}}(\mathcal{R},\boldsymbol{k},t') = \langle\boldsymbol{k}(t')|\boldsymbol{F}(t')\cdot\boldsymbol{r}|\phi_0\rangle \tag{16}$$

and recombination at time t

$$\boldsymbol{M}_{\mathrm{rec}}(\mathcal{R},\boldsymbol{k},t) = \langle\phi_0|\boldsymbol{v}|\boldsymbol{k}(t)\rangle. \tag{17}$$

B. State $|\Psi(t)\rangle$ and dipole velocity expectation value within the ASFA and SSFA

We now turn to a modification of the above procedure to account for the adiabatic motion in the ground state as accounted for in the ASFA. The starting point is analogous to Eq. (5) with an important difference. The dynamics of the active orbital is approximated by the essential state expansion

$$|\psi^a(t)\rangle = c_0^a(t)|\phi_0(t)\rangle \exp\left(-i\int_0^t E_0(t')dt'\right) + \int c_{\boldsymbol{k}}^a(t)|\boldsymbol{k}(t)\rangle \exp\left(-i\int_0^t E_{\boldsymbol{k}}(t')dt'\right)d\boldsymbol{k}, \tag{18}$$

where $|\phi_0(t)\rangle$ is the adiabatic ground state

$$f(t)|\phi_0(t)\rangle = E_0(t)|\phi_0(t)\rangle \tag{19}$$

with

$$f(t) = \frac{p^2}{2} + V^{\mathrm{HF}}(t) + \boldsymbol{F}(t)\cdot\boldsymbol{r}, \tag{20}$$

where $V^{\mathrm{HF}}(t)$ is the time-dependent HF potential including the interaction with the external field of the other electrons and the rest of the terms were defined in connection with Eq. (5). The adiabatic ground state of Eq. (19) is obtained by quantum chemistry methods [44]. The wave function is expanded in an atom-centered Gaussian basis and the HF equations in the presence of the field (19) are solved. This leads to a purely discrete bound state with a real-valued energy $E_0(t)$. In our notation we discriminate between the time-dependent adiabatic ground state, the time-dependent Fock operator, and the time-dependent HF potential and the corresponding time-independent quantities of the preceding section by the time argument.

To proceed, we consider $i\,\partial_t|\psi^a(t)\rangle = f(t)|\psi^a(t)\rangle$, project on $\langle\phi_0(t)|$ and $\langle\boldsymbol{k}(t)|$, and derive a set of linear coupled differential equations for $c_0^a(t)$ and $c_{\boldsymbol{k}}^a(t)$. These equations are simplified by the following approximations [see also the discussion after Eq. (12)]: (i) Depletion of the ground state is neglected, i.e., $c_0^a(t) \approx 1$; (ii) the overlap $\langle\boldsymbol{k}(t)|\phi_0(t)\rangle$ is set to zero; (iii) the continuum-continuum couplings are neglected, i.e., $\langle\boldsymbol{k}(t)|\boldsymbol{F}(t)\cdot\boldsymbol{r}|\boldsymbol{k}'(t)\rangle \approx 0$; and (iv) the terms $\langle\boldsymbol{k}(t)|V^{\mathrm{HF}}(t)|\boldsymbol{k}'(t)\rangle$ are neglected. The time evolution of the

continuum amplitude is then determined by

$$\dot{c}^a_{\boldsymbol{k}}(t) = -\langle \boldsymbol{k}(t)|\dot{\phi}_0(t)\rangle \exp\left(i\int_0^t (E_{\boldsymbol{k}}(t') - E_0(t'))dt'\right), \quad (21)$$

which is the ASFA equivalent of Eq. (13). The form of the coupling term on the rhs of Eq. (21) is a consequence of the adiabatic approximation for the ground state [45]. Integration of Eq. (21) gives

$$c^a_{\boldsymbol{k}}(t) = -\int_0^t \langle \boldsymbol{k}(t')|\dot{\phi}_0(t')\rangle \times \exp\left(i\int_0^{t'} (E_{\boldsymbol{k}}(t'') - E_0(t''))dt''\right)dt'. \quad (22)$$

The matrix element on the rhs of Eqs. (21) and (22) can be evaluated once the adiabatic ground state $|\phi_0(t)\rangle$ is known as a function of time and the state in Eq. (18) is thereby determined.

To connect with the standard SFA we rewrite the coupling $\langle \boldsymbol{k}(t')|\dot{\phi}_0(t')\rangle$ by partial integration of Eq. (22) and obtain

$$c^a_{\boldsymbol{k}}(t) = i\int_0^t \langle \boldsymbol{k}(t')|\boldsymbol{F}(t')\cdot\boldsymbol{r}|\phi_0(t')\rangle \times \exp\left(i\int_0^{t'} [E_{\boldsymbol{k}}(t'') - E_0(t'')]dt''\right)dt', \quad (23)$$

where we have used assumption (ii) above. The expression for the state in the ASFA then reads

$$|\psi^a(t)\rangle = |\phi_0(t)\rangle \exp\left(-i\int_0^t E_0(t')dt'\right) + i\int_0^t \int_0^t |\boldsymbol{k}(t)\rangle\langle \boldsymbol{k}(t')|\boldsymbol{F}(t')\cdot\boldsymbol{r}|\phi_0(t')\rangle \times \exp\left(-i\int_{t'}^t E_{\boldsymbol{k}}(t'')dt'' - i\int_0^{t'} E_0(t'')dt''\right)dt'd\boldsymbol{k}. \quad (24)$$

Compared with the standard SFA state of Eq. (14) there is a change of sign between the two terms in Eq. (24) and the presence of the adiabatic ground state and ground-state energy. The HHG spectrum is insensitive to such a phase change since it relates to the absolute square of the Fourier transform of the dipole velocity expectation value [Eq. (1)]. We cannot expect that Eq. (24) turns into Eq. (14) when orbital distortion is switched off. The reasons for this are the following. In the adiabatic approximation the presence of the external time-dependent field $\boldsymbol{F}(t)$ means that the adiabatic ground state $|\phi_0(t)\rangle$ (which depends on time via the instantaneous value of the field [Eq. (19)]) is different for each value of the field and therefore for each instant of time. The coupling to the continuum in the ASFA relies on this change over time as seen from Eq. (21). If there is no change in the field, there is no change in $|\phi_0(t)\rangle$ and there is no coupling. A change in $|\phi_0(t)\rangle$ is what we refer to as distortion: When $\boldsymbol{F}(t)$ changes, $|\phi_0(t)\rangle$ changes [Eq. (19)] and we have a distorted orbital. In the ASFA the ground-state orbital is always changing unless the field is constant. The field-free ground-state orbital used in the SFA corresponds to a vanishing external field. When the field is vanishing, there is no dynamics involving the continuum and no HHG. This argumentation shows that the SFA expression of Eq. (14) cannot be obtained from the ASFA in the limit where orbital distortion is switched off.

Equation (24) leads to the following expression for the expectation value of the dipole in the ASFA:

$$\langle \boldsymbol{v}^a(\mathcal{R},t)\rangle = i\int\int_0^t \boldsymbol{M}^a_{\rm rec}(\mathcal{R},\boldsymbol{k},t) \times \exp\left(-i\int_{t'}^t (E_{\boldsymbol{k}}(t'') - E_0(t''))dt''\right) \times M^a_{\rm ion}(\mathcal{R},\boldsymbol{k},t')dt'd\boldsymbol{k} + \text{c.c.}, \quad (25)$$

with ionization at time t' described by the matrix element

$$M^a_{\rm ion}(\mathcal{R},\boldsymbol{k},t') = \langle \boldsymbol{k}(t')|\boldsymbol{F}(t')\cdot\boldsymbol{r}|\phi_0(t')\rangle \quad (26)$$

and recombination at time t described by the matrix element

$$\boldsymbol{M}^a_{\rm rec}(\mathcal{R},\boldsymbol{k},t) = \langle \phi_0(t)|\boldsymbol{v}|\boldsymbol{k}(t)\rangle. \quad (27)$$

In both the SFA and the ASFA the $\langle\phi_0|\boldsymbol{v}|\phi_0\rangle$ and $\langle\phi_0(t)|\boldsymbol{v}|\phi_0(t)\rangle$ contributions to the HHG signal are neglected because these terms give rise to only low-order subthreshold harmonics. The SSFA [28–34,46] expressions for HHG can be obtained from the ASFA expressions for the matrix elements by the substitution rule $|\phi_0(t)\rangle \to |\phi_0\rangle$. The instantaneous field-dependent energy of the HOMO is denoted by $E_0(t)$ and using perturbation theory it is given by

$$E_0(t) = -I_p - \boldsymbol{\mu}\cdot\boldsymbol{F}(t) - \tfrac{1}{2}\boldsymbol{F}(t)^{\rm T}\underline{\underline{\boldsymbol{\alpha}}}\boldsymbol{F}(t), \quad (28)$$

with I_p the ionization potential of the HOMO, $\boldsymbol{\mu}$ the dipole of the HOMO, and $\underline{\underline{\boldsymbol{\alpha}}}$ its polarizability tensor.

III. RESULTS

Here we present our numerical results of HHG spectra for nonpolar CO_2 and polar N_2O molecules in the direction parallel to the polarization direction of the driving field. In the applications, we choose wavelengths and field strengths such that the adiabatic approximation for the ground state is justified and focus on situations where the harmonic yield is dominated by the signal from the HOMO. The latter restriction is ensured by using field parameters and molecular orientations similar to those used in previous experiments [10,47] where the minimum originated from the HOMO only. The HOMOs are obtained with quantum chemistry methods [44] within the HF approach using an augmented correlation-consistent polarized valence triple-ζ (aug-cc-pVTZ) basis set [48,49] for CO_2 and a valence triple-ζ basis set for N_2O. The HOMOs in the ASFA are calculated for every time step, i.e., every field value needed for an accurate evaluation of the integral in Eq. (25). Typically, the approach requires the diagonalization of the molecular Hamiltonian for 6000 different static fields. These orbitals and energies can be effectively achieved by parallel calculations on a cluster machine. Table I summarizes the parameters entering the calculations. Ionization potentials, dipole moments, and polarizabilities were found by fitting a second-order polynomial to the energy of the HOMO as a function of the field strength parallel and perpendicular to the molecular axis [see Eq. (28)]. The quantum chemistry code gives satisfying results for field strengths of interest for this work (see Ref. [51]).

TABLE I. Ionization potentials I_p, dipole moments parallel to the main molecular axis $\mu_{z,\mathrm{HOMO}}$, and polarizabilities perpendicular $\alpha_\perp$ and parallel $\alpha_{||}$ to the main molecular axis of the HOMOs of CO_2 and N_2O in atomic units. In the molecular frame with origin in the center of mass, the atoms are at the following positions: For CO_2, $z_C = -2.196$, $z_O = 0.0$, and $z_C = 2.196$, and for N_2O, $z_N = -2.267$, $z_N = -0.135$, and $z_O = 2.103$. The nuclear positions were chosen according to the experimental values of the National Institute of Standards and Technology database [50]. The values in the table were obtained by quantum chemistry methods [44] with aug-cc-pVTZ and valence triple-ζ basis sets.

Molecule	I_p	$\mu_{z,\mathrm{HOMO}}$	α_{HOMO}
CO_2	0.545	0.0	$\alpha_\perp = 3.40$
			$\alpha_{||} = -1.98$
N_2O	0.492	−0.023	$\alpha_\perp = 2.71$
			$\alpha_{||} = 7.154$

A. A molecule with low polarizability: CO_2

First we investigate the range of validity of the approach presented in Sec. II B by studying HHG spectra from CO_2, which is one of the most widely studied molecules with HHG techniques [10,14,23,24,40,47,52,53]. It is well known that the HHG spectrum from CO_2 exhibits a very distinct minimum [10,14,40,47]. The minimum, though, has a complex origin. Depending on field parameters and orientation of the molecule, the minimum may be caused by destructive interference between signals from different orbitals [14,40,47] or, alternatively, by destructive interference from the two outer O centers [10,47]. One of the key features determining the importance of the given type of the minimum is the binding energy of molecular orbitals compared to the frequency of the laser light. For increasing wavelength, i.e., decreasing photon energy, more photons are needed to couple different orbitals. Therefore, as demonstrated in Ref. [47], it becomes less probable to obtain a signal from lower-lying orbitals as the wavelength increases.

We focus on the two-center interference minimum from the HOMO, choosing field parameters and orientation for which it was experimentally shown [10,47] that the signal from lower-lying orbitals does not influence the minimum. Figure 1 depicts HHG spectra from the HOMO of CO_2 aligned at $\beta = 45^\circ$ with respect to the linear polarization of the driving field. The molecule is subject to an eleven-cycle pulse of 1460 nm, with two optical cycles used for ramp up and down the field. The laser intensity varies from 1×10^{14} to 3×10^{14} W/cm^2. The figure shows a deep distinct minimum at around 62 eV, which, in view of the energy relation

$$\omega = \frac{\boldsymbol{k}^2}{2} + I_p, \tag{29}$$

where ω is the photon energy, $\boldsymbol{k}$ is the electron momentum, and I_p is the ionization potential, corresponds to an energy of 47 eV of the recombining electron. For intensities between 1×10^{14} and 2×10^{14} W/cm^2 this agrees with experimental data [10] obtained for similar field parameters and orientations. The minimum exists even for an intensity of 3×10^{14} W/cm^2. For all three intensities the spectral shapes obtained using the ASFA

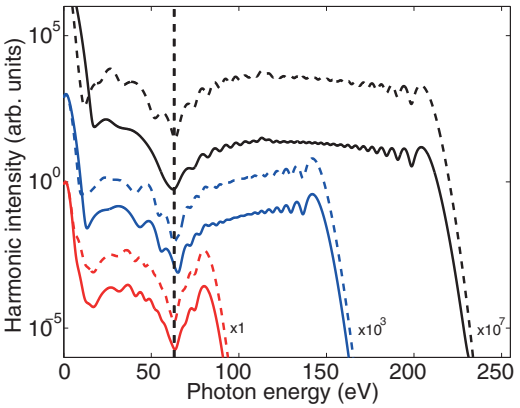

FIG. 1. (Color online) The HHG spectra for CO_2 normalized to the highest harmonic intensity for each curve. The spectra have been smoothed out with a Gaussian distribution with a full width at half maximum of four harmonics. Solid (dashed) lines show the results of the ASFA (SSFA). The lower two (red) lines correspond to an intensity of 1×10^{14} W/cm^2. The middle two (blue) lines correspond to an intensity of 2×10^{14} W/cm^2. The upper two (black) lines correspond to an intensity of 3×10^{14} W/cm^2. The molecule is aligned at $\beta = 45^\circ$ with respect to the linear polarization of an eleven-cycle pulse of 1460 nm, with two optical cycles used for ramp-up and -down. The lines are multiplied by the factors shown.

(solid lines in Fig. 1) agree with the shapes obtained using the SSFA [28] (dashed lines in Fig. 1). This agreement is a consequence of a low degree of field distortion of the HOMO of CO_2, as reflected by the relatively small polarizability of the HOMO (see Table I).

An analysis of recombination matrix elements (RMEs) (see, e.g., Refs. [35,54,55]) provides insight into the recombination process at a given instant of time, i.e., at a given field strength. Such an analysis allows, for instance, the determination of the weak-field region [35], where the field is so weak that the field distortion of orbitals is small enough to observe features of the HHG spectrum that are typical for undistorted orbitals. In the HHG process emission of harmonics happens almost throughout the whole pulse duration and consequently at many different field strengths. Therefore, we consider the recombination at each frequency during the whole process. Calculating time-averaged RMEs for each harmonic weighted with the emission yield allows us to elucidate the main contributions to the RMEs for each harmonic. Within the ASFA the averaged RME (ARME) for the ith center in the molecule is

$$R_i(\omega) = \frac{\int_{-\infty}^{\infty} P(\omega,t)\langle\phi_0^{(i)}(t)|\boldsymbol{v}|\boldsymbol{k}(t)\rangle dt}{\int_{-\infty}^{\infty} P(\omega,t)dt}, \tag{30}$$

where $P(\omega,t)$ is the emission yield at the photon energy ω at time t obtained from a time profile analysis (Gabor transform) [56]. The part of the adiabatic ground-state orbital centered on the ith atom calculated in the presence of the field is given by $|\phi_0^{(i)}(t)\rangle$ and is readily retrieved from the atom-centered Gaussian basis used in the quantum chemistry calculation [44].

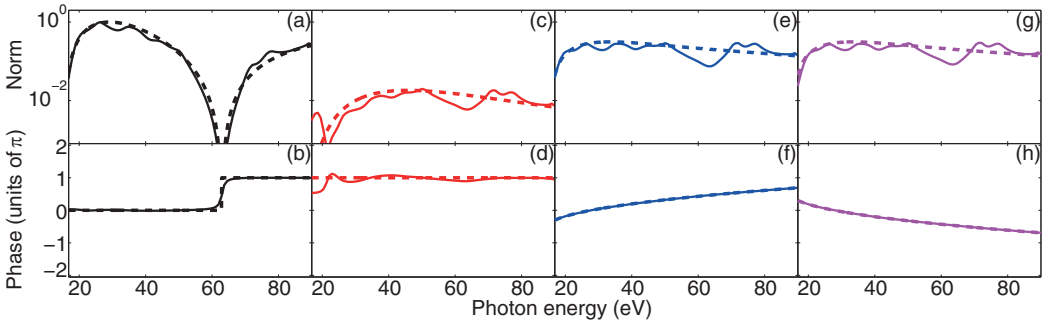

FIG. 2. (Color online) Norms and phases of ARMEs [Eqs. (30) and (31)] normalized to the peak value of the molecular ARMEs for CO_2 aligned at $\beta = 45^\circ$ with respect to the linear polarization of an eleven-cycle pulse of 1460 nm, with two optical cycles for ramp-up and -down, and an intensity of 1×10^{14} W/cm^2. Solid (dashed) lines show ASFA (SSFA) ARMEs for (a) norms and (b) phases of the molecular ARMEs, (c) norms and (d) phases of ARMEs from the C atom, (e) norms and (f) phases of ARMEs from the O atom at the negative z axis in the molecular frame (see Table I), and (g) norms and (h) phases of ARMEs from the O atom at the positive z axis in the molecular frame.

The molecular ARME is the sum of ARMEs from all centers

$$R(\omega) = \sum_i R_i(\omega). \tag{31}$$

The ARMEs within the SSFA are obtained from Eqs. (30) and (31) using the field-free ground-state orbital $|\phi_0^{(i)}\rangle$. The ARMEs within the SSFA equal those in the SFA since the field-free orbital is used and there is no energy phase in the ARME.

A decomposition of the full molecular ARMEs into the ARMEs of the individual centers allows us to understand the origin of the interference minimum. Averaged RMEs normalized to their peak value are shown in Figs. 2 and 3. Here solid (dashed) lines depict ASFA (SSFA) ARMEs. Figure 2 shows norms and phases of ARMEs at 1×10^{14} W/cm^2. Because the single-center ASFA and SSFA ARMEs are very similar [Figs. 2(c)–2(h)] for all photon energies, both norms and phases of the ASFA and SSFA molecular ARMEs fall almost on top of each other [Figs. 2(a) and 2(b)]. Therefore, the HHG spectrum using the ASFA, that is, inclusion of the field-distorted orbitals in Eqs. (26) and (27), does not introduce any new features compared to the SSFA spectrum (Fig. 1). Figure 2(f) and 2(h) show that the ARMEs from the two O atoms are approximately π out of phase at the position of the minimum in the HHG spectrum at photon energies ≈62 eV. The corresponding norms in Figs. 2(e) and 2(g) are of equal magnitude. As a result, almost full destructive interference between ARMEs from the O atoms takes place, resulting in a deep minimum around 62 eV in Fig. 2(a) and a corresponding phase jump in Fig. 2(b) of the molecular ARME for both the ASFA and SSFA [see Eq. (31)]. The influence of the middle C atom is negligible in the creation of this structure [Figs. 2(c) and 2(d)]. This is because the norm of its ARME is almost two orders of magnitude smaller than the norms of the ARMEs from the O atoms [compare Fig. 2(c) with Figs. 2(e) and 2(g)]. It is then justified to name it the two-center interference minimum even though, formally, all three centers take part in the process [see Eq. (31)].

Even for the stronger field with 3×10^{14} W/cm^2 (Fig. 3), ASFA and SSFA ARMEs agree very well. Hence the same conclusions as in the previous paragraph can be drawn. Moreover, the conclusions should not change after taking into account an imperfect alignment distribution around 45°. The contribution to the HHG spectrum decreases with increasing deviation of the alignment angle away from $\beta = 45^\circ$. The decrease in the signal is caused by the decrease in the ionization yield and by the shape of the alignment distribution, which peaks at 45°. As a result, molecules aligned around $\beta = 45^\circ$ contribute most to the creation of the HHG spectrum

The small discrepancy between ASFA and SSFA ARMEs shows that the CO_2 molecule is robust to distortion by a strong external field and therefore one may safely assume that features typical for field-free orbitals can be retrieved from HHG spectra for this molecule and subsequently used for, e.g., field-free orbital tomography for this particular molecule [6,10]. Orbital imaging via, e.g., laser-induced electron diffraction [57] should also remain unaffected by the field-induced orbital distortion.

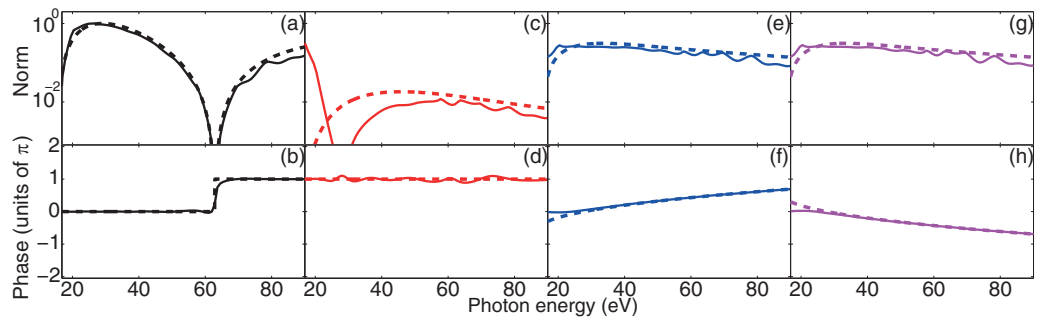

FIG. 3. (Color online) Same as Fig. 2 but for an intensity of 3×10^{14} W/cm^2.

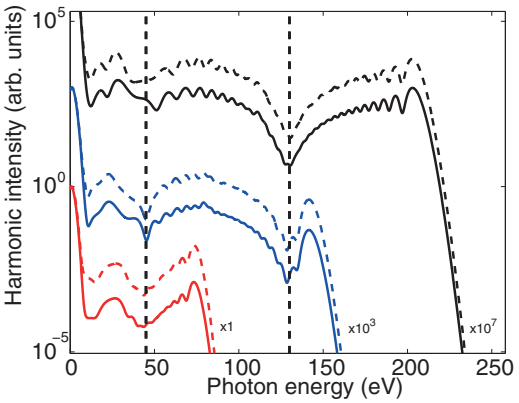

FIG. 4. (Color online) The HHG spectra for N_2O normalized to the highest harmonic intensity for each curve. The spectra have been smoothed out with a Gaussian distribution with a full width at half maximum of four harmonics. Solid (dashed) lines show the results of the ASFA (SSFA). The lower two (red) lines correspond to an intensity of 0.93×10^{14} W/cm^2. The middle two (blue) lines correspond to an intensity of 2×10^{14} W/cm^2. The upper two (black) lines correspond to an intensity of 3×10^{14} W/cm^2. The molecule is aligned at $\beta = 10^\circ$ with respect to the linear polarization of an eleven-cycle pulse of 1460 nm, with two optical cycles used for ramp-up and -down. The lines are multiplied by the factors shown.

B. A molecule with intermediate polarizability: N_2O

In this section we present results for HHG from N_2O (Table I) where the HOMO has a polarizability greater than that of the HOMO of CO_2 but at the same time not large enough for the two-center interference minimum to vanish due to orbital distortion for the orientations and intensities used in Ref. [47]. We expect to observe a changing influence of field distortion on the two-center interference minimum when varying the laser intensity. We study the HHG spectra from N_2O oriented at $\beta = 10^\circ$ with respect to the linear polarization of the driving eleven-cycle pulse with a wavelength of 1460 nm and with a trapezoidal envelope. The $\beta = 10^\circ$ corresponds to a geometry with the O atom having a positive projection on the laboratory-fixed z axis. The dipole of the HOMO points from the O atom and towards the N atoms (Table I).

Figure 4 shows HHG spectra for 0.93×10^{14} W/cm^2 (used in Ref. [47]), 2×10^{14} W/cm^2, and 3×10^{14} W/cm^2. Both the ASFA (solid lines) and the SSFA (dashed lines) show pronounced minima at a photon energy around 45 eV. The position of the minimum differs by 8 eV from the experimental data [47] obtained using similar laser parameters. Although not central for our discussion of orbital distortion and polarizability effects, we mention a possible reason for this discrepancy. When the polarization vector of the driving field is parallel to the nodal plane of the HOMO ($\beta = 0^\circ$) the HHG signal is strongly suppressed. Even small deviations from this orientation would result in a strong increase in the signal. This tendency holds up to $\beta = 45^\circ$, where the ionization rate reaches its maximum [47]. The two-center interference minimum moves to higher energies with increasing orientation angle [21,22]. Therefore, in the experiment, even with a relatively high degree of orientation, the dominant contribution to the spectrum may originate from molecules far from the average experimental orientation angle. This is a possible reason why the position of the minimum in the experiment appears at higher photon energies than predicted by our model for fixed $\beta = 10^\circ$.

For laser intensities of 0.93×10^{14} and 2×10^{14} W/cm^2 the depth and shape of the interference minimum at ≈45 eV is comparable in the ASFA and SSFA (Fig. 4). Molecular and single-center ARMEs for a laser intensity of 0.93×10^{14} W/cm^2 are depicted in Fig. 5. The phases obtained within the ASFA (solid lines) and the SSFA (dashed lines) agree very well in all cases [Figs. 5(b), 5(d), 5(f), and 5(h)]. Figures 5(f) and 5(h) show that the ARMEs of the middle N and the O atom are in phase at photon energies around 45 eV, leading to constructive interference between these two centers. Figure 5(d) shows that the ARME of the outermost N atom is approximately π out of phase at the position of the minimum, resulting in destructive interference between the contribution from this center and the former two. A comparison of the norms of ARMEs obtained by the SSFA [Figs. 5(c), 5(e), and 5(g)] shows that only the outermost atoms [Figs. 5(c) and 5(g)] are relevant for the overall molecular ARME since the norm of the ARME of the middle center [Fig. 5(e)] is approximately one order of magnitude lower. The relatively large difference in norms of the ARMEs from the outermost N atom [Fig. 5(c)] and the O atom [Fig. 5(g)] means that the

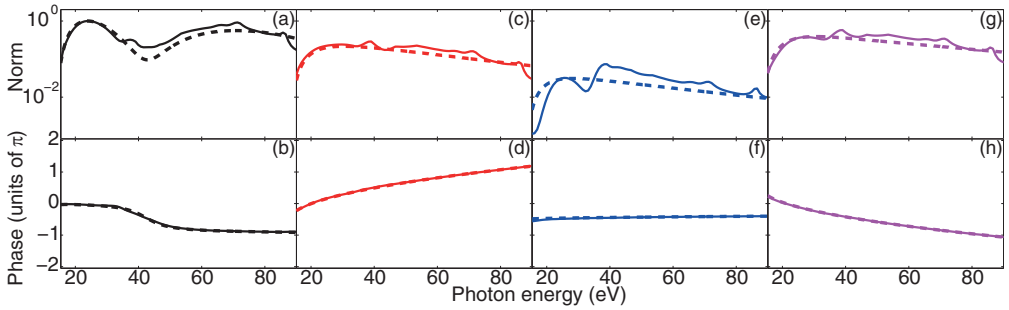

FIG. 5. (Color online) Norms and phases of ARMEs [Eqs. (30) and (31)] normalized to the peak value of the molecular ARMEs for N_2O aligned at $\beta = 10^\circ$ with respect to the linear polarization of an eleven-cycle pulse of 1460 nm, with two optical cycles for ramp-up and -down and an intensity of 0.93×10^{14} W/cm^2. Solid (dashed) lines show ASFA (SSFA) ARMEs for (a) norms and (b) phases of the molecular ARMEs, (c) norms and (d) phases of ARMEs from the outermost N atom, (e) norms and (f) phases of ARMEs from the middle N atom, and (g) norms and (h) phases of ARMEs from the O atom.

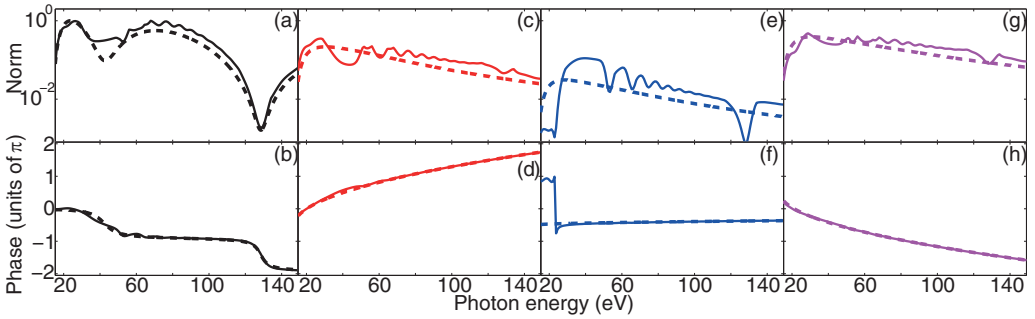

FIG. 6. (Color online) Same as Fig. 5 but for an intensity of 3×10^{14} W/cm^2.

destructive interference in the case of N_2O is less pronounced than in the case of CO_2 [compare minima in Figs. 5(a) and 2(a)]. Note that the phase jump of the molecular ARME is also not as pronounced as in the CO_2 case [compare Figs. 5(b) and 2(b)]. The situation is somewhat different in the results of the ASFA. The norms of the ARMEs of the two outermost atoms follow the results of the SSFA [Figs. 5(c) and 5(g)]. The norm of the middle one, on the other hand, differs slightly and increases close to a photon energy of ≈45 eV [Fig. 5(e)]. As a consequence, the influence of the middle center on the molecular ARME, though weak, cannot be neglected and the minimum in the ASFA is less pronounced [Fig. 5(a)].

For a higher intensity of 3×10^{14} W/cm^2 (Fig. 6) the phases in the ASFA ARMEs (solid lines) still fall on top of the SSFA ARMEs phases (dashed lines) for most of the energy range [Figs. 6(d), 6(f), and 6(h)]. Therefore, as in the low-intensity case, constructive interference occurs between ARMEs from the middle N and the O atom at a photon energy around 45 eV along with destructive interference between these two and the ARME from the outermost N atom. The norms of the ASFA and SSFA ARMEs of the O center are very similar [Fig. 6(g)]. The norms of ASFA ARMEs from the N atoms, however, deviate from the SSFA results [Figs. 6(c) and 6(e)]. The deviation is largest at photon energies between 30 and 50 eV, i.e., in the energy range where the minimum in the molecular ARME appears [Fig. 6(a)]. The norm of the ASFA ARME from the outer N atom [Fig. 6(c)] has a local minimum around 45 eV. The norm of the ASFA ARME from the middle N atom [Fig. 6(e)], on the other hand, is markedly higher than the SSFA norm in this energy range. Therefore, the influence of the middle center on the molecular ARME becomes important. In the close vicinity of the minimum the ARME from the middle center has a slightly larger norm than that from the outer N atom [compare Figs. 6(c) and 6(e)]. As a consequence, almost total destructive interference occurs between the ASFA ARMEs from the N atoms and therefore the molecular ARME follows quite closely the ARME from the O center. This results in a shallowing of the minimum in the molecular ARME as compared to the SSFA molecular ARME [Fig. 6(a)].

In the creation of the first-order interference minimum of Fig. 6(a), all three centers contribute, therefore this is a three-center interference minimum. Comparing Figs. 5 and 6, we therefore see that the importance of each center in the creation of the interference minimum varies with intensity. The second-order minimum in the HHG spectrum at photon energies around 130 eV (see Fig. 4) is due to destructive interference between ARMEs from the outermost atoms since

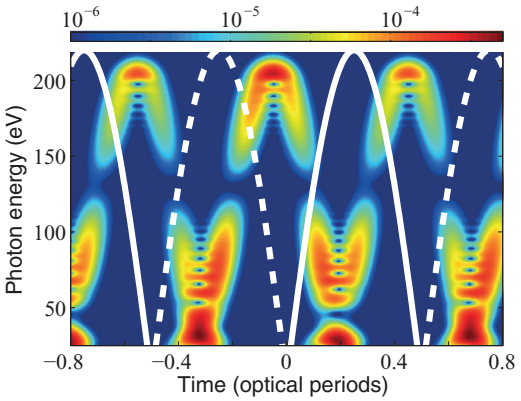

FIG. 7. (Color online) Time profile analysis (Gabor transform) within the ASFA from the HOMO of N_2O subject to an eleven-cycle pulse of 1460 nm, with two optical cycles used for ramp-up and -down, with an intensity of 3×10^{14} W/cm^2 and orientation angle $\beta = 10^\circ$ with respect to the linear polarization of the driving field. The curves show positive (white solid lines) and negative (white dashed lines) values of the laser field at the recombination time.

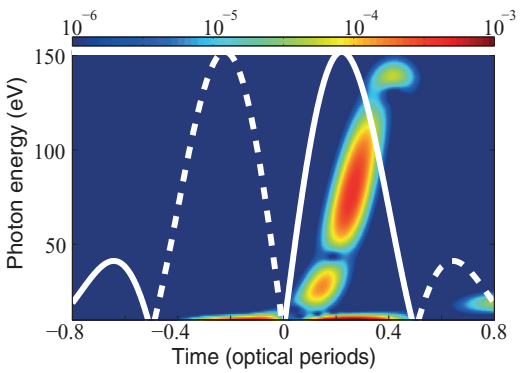

FIG. 8. (Color online) Time profile analysis (Gabor transform) of the short trajectories within the ASFA from the HOMO of N_2O aligned at $\beta = 10^\circ$ with respect to the linear polarization of the field [Eq. (33)] of a two-cycle pulse of 1460 nm, with $\phi_{CEP} = -\pi/2$ and peak field strength $F_0 = 0.0924$ a.u. The curves show positive (white solid lines) and negative (white dashed lines) values of the laser field at the recombination time.

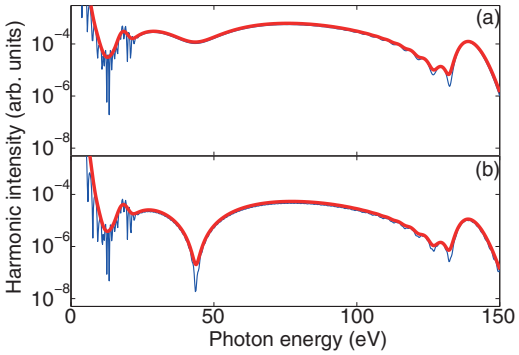

FIG. 9. (Color online) The HHG spectra of the short trajectories [thin (blue) lines] and corresponding spectra that have been smoothed out [thick (red) lines] with a Gaussian distribution with a full width at half maximum of four harmonics, for N_2O aligned at $\beta = 10^\circ$ with respect to the linear polarization of the field of a two-cycle pulse of 1460 nm, with $\phi_{CEP} = -\pi/2$ and peak field strength $F_0 = 0.0924$ a.u. [Eq. (33)]: (a) the HHG spectrum using the SSFA [28] and (b) the HHG spectrum using the ASFA. Compared to the long-pulse case, the position of the minimum has shifted slightly from 45 eV to 43.5 eV.

the ARME from the middle N atom is more than one order of magnitude smaller [see Figs. 6(d), 6(h), and 6(f)].

The N_2O molecule has no inversion symmetry and possesses a permanent dipole moment allowing for molecular orientation [58]. For polar molecules the response to the driving laser field depends on the instantaneous direction and value of the field as a consequence of the Stark-shifted energy levels [see Eq. (28)] and orbital shapes [46,59,60]. One way to gain insight into such behavior in connection with HHG is by considering a time profile analysis (Gabor transform) of the signal (see Ref. [56]). Figure 7 shows such a Gabor transform. The first prominent feature in Fig. 7, which has already been reported previously [28,31,32], is the difference in the overall strength of the signal for recombining electrons that were detached in half cycles with different field directions. This can be seen in Fig. 7 since emission of the most energetic harmonics happens roughly 2/3 of an optical cycle after electron detachment. Harmonics that belong to the short (long) trajectory are emitted by the recombination of electrons detached less (more) than 2/3 of an optical cycle before [61]. Hence the detachment of the electrons that recombine around time 0 (from around −0.3 to 0.2) in Fig. 7 took place for positive values of the field [solid (dashed) white lines show positive (negative) fields]. The dipole for N_2O points from O to N (Table I) and for the orientation $\beta = 10^\circ$ has its projection along the negative laboratory-fixed z axis. This means that the projection of the molecular dipole moment was antiparallel to the field ($\boldsymbol{F} \cdot \boldsymbol{\mu} < 0$, i.e., $\boldsymbol{F} = F\hat{z}$) at the time of detachment, hence the electrons were less tightly bound due to the Stark shift, i.e., more readily detached [see Eq. (28)]. Electrons recombining between times around −0.8 to −0.3 and between around 0.2 to 0.7 (Fig. 7) were detached for negative values of the field. In this case the projection of the molecular dipole moment was parallel to the field ($\boldsymbol{F} \cdot \boldsymbol{\mu} > 0$, i.e., $\boldsymbol{F} = -F\hat{z}$) at the time of detachment and the electrons were more tightly bound by the Stark shift compared to the field-free case and were consequently less easily detached. This Stark-shift-induced asymmetry in the detachment relates to the difference in the strength of the signal for times around −0.3 to 0.2 compared with times around −0.8 to −0.3 and 0.2 to 0.7.

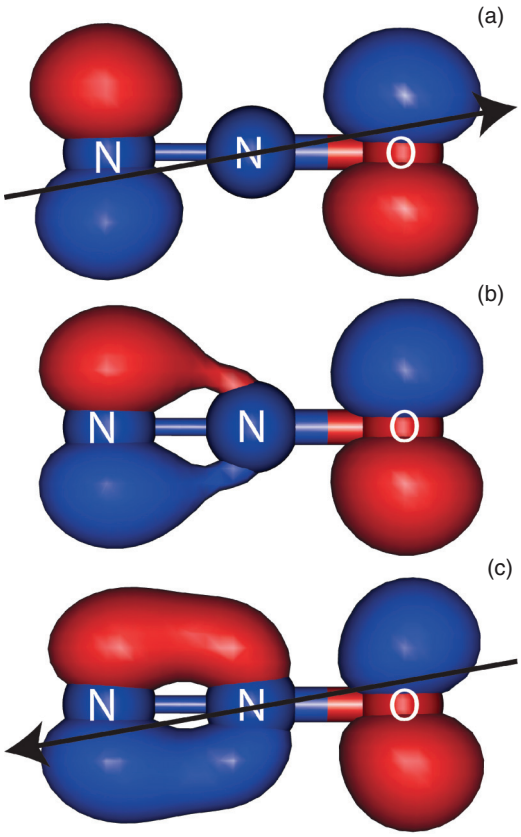

FIG. 10. (Color online) (a) Field-distorted HOMO of N_2O for $F = 0.08$ a.u. (b) Field-free HOMO of N_2O. (c) Field-distorted HOMO of N_2O for $F = -0.08$ a.u. Black arrows in (a) and (c) show the instantaneous field direction. The isocontour surface value is 0.1.

The second important feature of Fig. 7 is the difference in the strength of different frequency components of the emitted signal for positive and negative fields at the instant of recombination. Figure 7 shows that for electrons recombining for positive fields [solid (white) line] the two-center interference minimum (for photon energies around 45 eV) is very pronounced. On the other hand, this minimum vanishes when HHG emission of light happens for negative fields [dashed (white) line]. A detailed discussion of this phenomenon is given in the next section.

C. Short pulse

As seen in Sec. III B, the oriented polar target of N_2O gives rise to an asymmetry in the emission of HHG from positive and negative half cycles. For further investigation of this phenomenon we turn our attention to the short trajectories and such short pulses that the relevant ionization and recombination events can be confined to only one half cycle each. In this way the projection of the electric field on

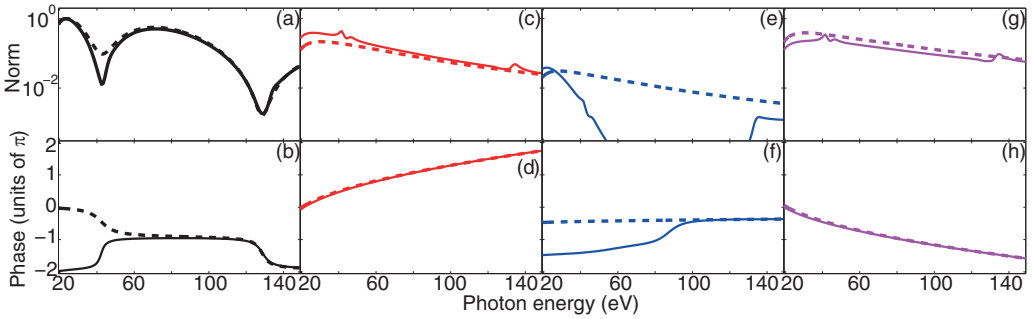

FIG. 11. (Color online) Norms and phases of ARMEs [Eqs. (30) and (31)] of the short trajectories normalized to the peak value of the molecular ARMEs for N_2O aligned at $\beta = 10^\circ$ with respect to the linear polarization of a two-cycle pulse of 1460 nm, with $\phi_{\rm CEP} = -\pi/2$ and peak field strength $F_0 = 0.0924$ a.u. [Eq. (33)]. Solid (dashed) lines show ASFA (SSFA) ARMEs for (a) norms and (b) phases of the molecular ARMEs, (c) norms and (d) phases of ARMEs from the outermost N atom, (e) norms and (f) phases of ARMEs from the middle N atom, and (g) norms and (h) phases of ARMEs from the O atom.

the molecular dipole moment is always either only positive or only negative during ionization and recombination. Such a situation allows an accurate study of the HHG spectra for opposite orientations and reveals a strong dependence on the orientation of the polar molecule.

The short-trajectory part is extracted with the help of a window function

$$f(t) = 1 - \left(\exp\left[\frac{t' - t + 0.99 \times 2T/3}{0.03T} \right] + 1 \right)^{-1}, \quad (32)$$

with t' the ionization time and T the optical period. The dipole velocity expectation value [see Eq. (25)] is multiplied by $f(t)$ and then this product is used to obtain the HHG spectra of Figs. 9 and 13 via the Fourier transform and the time profile analysis of Figs. 8 and 12 via the Gabor transform. The exact form of the window function is chosen such that the near cutoff harmonics from the long trajectories also contribute and so this way we make sure that nothing of the short-trajectory contribution is removed

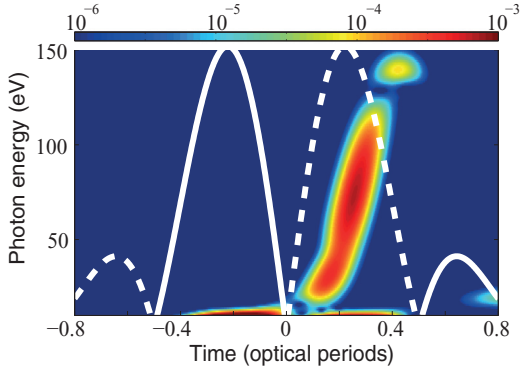

FIG. 12. (Color online) Time profile analysis (Gabor transform) of the short trajectories within the ASFA from the HOMO of N_2O aligned at $\beta = 10^\circ$ with respect to the linear polarization of the field [Eq. (33)] of a two-cycle pulse of 1460 nm, with $\phi_{\rm CEP} = \pi/2$ and peak field strength $F_0 = 0.0924$ a.u. The curves show positive (white solid lines) and negative (white dashed lines) values of the laser field at the recombination time.

We performed calculations of HHG from N_2O oriented at $\beta = 10^\circ$ with respect to the polarization of the short pulse

$$\boldsymbol{F}(t) = \begin{cases} \boldsymbol{\epsilon} F_0 \cos(\omega_L t + \phi_{\rm CEP}) \cos^2\left(\frac{\pi}{NT} t\right) & \text{for } |t| < \frac{NT}{2} \\ 0 & \text{otherwise,} \end{cases} \quad (33)$$

where $F_0 = 0.0924$ is the peak field strength, $\omega_L = 0.0312$ is the carrier frequency corresponding to a wavelength of 1460 nm, $N = 2$ is the number of cycles, and $T = 201.3$ is the optical period. Calculations were performed for carrier-envelope phases $\phi_{\rm CEP} = \pm\pi/2$, where the main part of ionization and recombination occurs during one half cycle each.

For $\phi_{\rm CEP} = -\pi/2$ the main ionization event occurs for negative field values, i.e., $\boldsymbol{F} \cdot \boldsymbol{\mu} > 0$ (see Fig. 8 and the discussion of detachment and recombination in the previous section). The Stark shift increases the ionization potential during this main ionization event. As a consequence, a smaller part of the molecular orbital is detached compared to the case with no Stark shift included. Figure 8 shows that recombination of the short trajectories happens for positive field values. The spectra obtained using the SSFA and the ASFA [see Figs. 9(a) and 9(b), respectively] agree well with each other for the chosen orientation and field parameters except that the first-order minimum at ≈43.5 eV is much deeper in the ASFA than in the SSFA. This can be understood by looking at the shape of the HOMO when distorted by the field resulting in HHG emission of photons of energy around 43.5 eV. Figures 10(a) and 10(b) show the field-distorted and field-free HOMOs, respectively. For strong fields pointing from N to O, the electron density of the middle N shifts towards the outermost N, resulting in a negligible effect of the middle N atom in the interference in the recombination step. At the same time the electron cloud has almost identical weight on both outermost atoms, making the two-center interference even more pronounced than in the field-free case. An analysis of the ARMEs depicted in Fig. 11 supports these conclusions. In Fig. 11 solid (dashed) lines show norms and phases of ARMEs obtained with the ASFA (SSFA). Figure 11(e) shows that the orbital distortion in the ASFA strongly suppresses the norm of the ARMEs from the middle N atom, as expected from the orbitals in Fig. 10. This means that the molecular ARMEs are

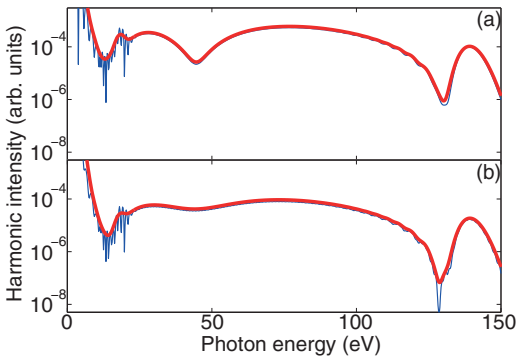

FIG. 13. (Color online) The HHG spectra of the short trajectories [thin (blue) lines] and corresponding spectra that have been smoothed out [thick (red) lines] with a Gaussian distribution with a full width at half maximum of four harmonics, for N_2O aligned at $\beta = 10^\circ$ with respect to the linear polarization of a two-cycle pulse of 1460 nm, with $\phi_{CEP} = \pi/2$ and peak field strength $F_0 = 0.0924$ a.u. [Eq. (33)]: (a) the HHG spectrum using the SSFA [28] and (b) the HHG spectrum using the ASFA.

formed from the ARMEs from the outermost N and the O atom only. Figures 11(d) and 11(h) show that the phases of the ASFA ARMEs fall on top of the SSFA ARMEs phases and agree well with the phases obtained for long-pulse cases (Figs. 5 and 6). For photon energies around 43.5 eV the phase difference between the ARME of the outermost N atom and the O atom reaches π leading to destructive interference between the ARMEs of comparable norms [Figs. 11(c) and 11(g)] and as a result to a deep minimum in Fig. 11(a).

When $\phi_{CEP} = \pi/2$, ionization occurs almost exclusively for positive field values, i.e., $\boldsymbol{F} \cdot \boldsymbol{\mu} < 0$ (see Fig. 12). In this case the ionization potential is decreased by the Stark shift compared with the field-free case and ionization occurs more readily. For this ϕ_{CEP}, short-trajectory electrons recombine for negative field values. The HHG spectra depicted in Fig. 13 show that the first-order interference minimum essentially vanishes in the ASFA [Fig. 13(b)], whereas the minimum is clearly visible in the SSFA [Fig. 13(a)]. A strong electric field, acting on N_2O, pointing from O to N drives the electron cloud from the outermost N atom to the middle N atom [see Figs. 10(b) and 10(c)]. This increases the importance of the middle center in the recombination process and at the same time slightly decreases the electron density centered on the outer N atom. The ASFA ARMEs shown in Fig. 14 (solid lines) reveal the enhanced importance of the middle center with respect to SSFA ARMEs (dashed lines) [Fig. 14(e)]. The norm of its ARME is comparable with the norm of the ARME from the outer N atom [Fig. 14(c)]. As a result, in the vicinity of the first-order interference minimum (at photon energy around 43.5 eV), the destructive interference between these two takes place [compare the phases in Figs. 14(d) and 14(f)] and hence the norm of the molecular ARME [Fig. 14(a)] is mainly determined by the norm of the ARME of the O atom in this energy range [Fig. 14(g)]. Consequently, almost a full vanishing of the interference minimum is observed in Fig. 13(b).

The window function in the Gabor transforms used in our work had a full width at half maximum (FWHM) of 0.1 times the optical cycle. We have checked the robustness of our conclusions, regarding the ARMEs, with respect to changes of the FWHM of this window function. The ARMEs obtained using the Gabor transform with a FWHM of 0.05 and 0.2 times the optical cycle (not presented) are similar to the ARMEs obtained using a FWHM of 0.1 times the optical cycle and hence the conclusions are insensitive to the FWHM.

Using state of the art techniques for molecular orientation [58] and pulse shaping [62], one should be able to perform an experiment for which the difference in HHG spectra, from opposite orientations, could be observed in terms of a change in the minimum as a supplement to the presence of even harmonics [28,63–65]. An ensemble of imperfectly oriented molecules typical for experiments should not affect the conclusions. The parallel component of the polarizability of N_2O is much larger than the perpendicular one (see Table I). Consequently, the HOMO of a molecule, driven by a field oriented such that β lies within a relatively large range around 10°, experiences distortion mainly along the main molecular axis. As a result, most of the HOMOs from the ensemble undergo similar distortion when driven by the laser field given by Eq. (33). At the recombination time for which short-trajectory harmonics from the vicinity of the minimum

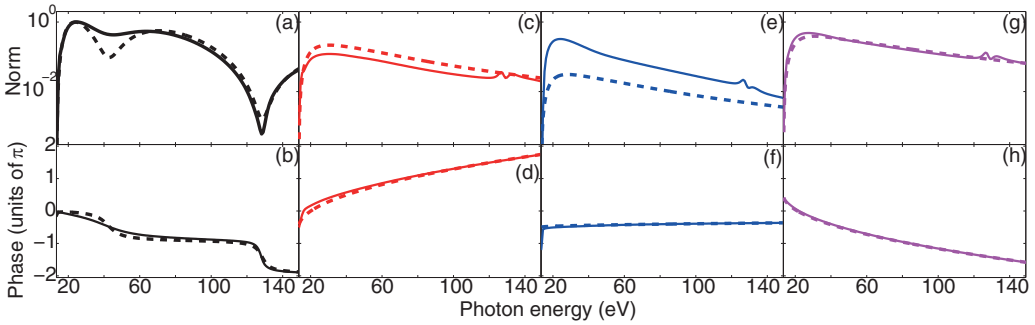

FIG. 14. (Color online) Norms and phases of ARMEs [Eqs. (30) and (31)] of the short trajectories normalized to the peak value of the molecular ARMEs for N_2O aligned at $\beta = 10^\circ$ with respect to the linear polarization of a two-cycle pulse of 1460 nm, with $\phi_{CEP} = \pi/2$ and peak field strength $F_0 = 0.0924$ a.u. [Eq. (33)]. Solid (dashed) lines show ASFA (SSFA) ARMEs for (a) norms and (b) phases of the molecular ARMEs, (c) norms and (d) phases of ARMEs from the outermost N atom, (e) norms and (f) phases of ARMEs from the middle N atom, and (g) norms and (h) phases of ARMEs from the O atom.

are born the HOMOs exhibit the following behavior. For the field with $\phi_{\mathrm{CEP}} = -\pi/2$ most of the HOMOs consist of two distinct centers, similarly to Fig. 10(a). When the ensemble is driven by the field with $\phi_{\mathrm{CEP}} = \pi/2$ most of the HOMOs exhibit three centers, as depicted in Fig. 10(c). Therefore, the HHG spectrum from the imperfectly oriented ensemble of molecules should reveal similar features, as in the cases presented in Figs. 9 and 13.

IV. CONCLUSION

We have investigated the effects of field-induced orbitals distortion within the framework of the ASFA and SSFA for HHG. We have performed calculations for molecules with different polarizabilities and presented results that show that the polarizability is a good measure of the effect of orbital distortion of a molecule in an external laser field.

The very good agreement between the experiment [10] and the calculations for CO_2 supported the used method. Negligible orbital distortion shown by the calculations allows us to conclude that HHG spectra from the HOMO of CO_2 can, e.g., reveal field-free orbital features.

Due to the moderate polarizability of N_2O, the response of the HOMO to the field varies with the field intensity. This implies that the depth, position, and number of centers taking part in the creation of the interference minimum in the HHG spectrum vary with the intensity.

When a molecule with no inversion symmetry is used as a target in the HHG process the spectrum emitted in half cycles with fields pointing in opposite directions is different. The difference occurs not only in the strength of the signal, as it has been shown before [28], but also in the shape of the emitted signal. We have reported a significant difference in the HHG spectrum from opposite orientations by using phase-stabilized few-cycle pulses. In particular, we showed that the observation of the two-center interference minimum depends on the field direction during the main recombination event.

ACKNOWLEDGMENTS

We thank Dr. Sebastian Bauch for useful comments and suggestions. This work was supported by the Danish Center for Scientific Computation, the Danish Natural Science Research Council, and an ERC Starting Grant (Project No. 277767, TDMET).

[1] A. Rundquist, C. G. Durfee, Z. Chang, C. Herne, S. Backus, M. M. Murnane, and H. C. Kapteyn, Science **280**, 1412 (1998).
[2] S. Baker, J. S. Robinson, C. A. Haworth, H. Teng, R. A. Smith, C. C. Chirilă, M. Lein, J. W. G. Tisch, and J. P. Marangos, Science **312**, 424 (2006).
[3] S. Baker, J. S. Robinson, M. Lein, C. C. Chirilă, R. Torres, H. C. Bandulet, D. Comtois, J. C. Kieffer, D. M. Villeneuve, J. W. G. Tisch *et al.*, Phys. Rev. Lett. **101**, 053901 (2008).
[4] W. Li, X. Zhou, R. Lock, S. Patchkovskii, A. Stolow, H. C. Kapteyn, and M. M. Murnane, Science **322**, 1207 (2008).
[5] X. Zhou, R. Lock, W. Li, N. Wagner, M. M. Murnane, and H. C. Kapteyn, Phys. Rev. Lett. **100**, 073902 (2008).
[6] J. Itatani, J. Levesque, D. Zeidler, H. Niikura, H. Pépin, J. C. Kieffer, P. B. Corkum, and D. M. Villeneuve, Nature (London) **432**, 867 (2004).
[7] S. Patchkovskii, Z. Zhao, T. Brabec, and D. M. Villeneuve, Phys. Rev. Lett. **97**, 123003 (2006).
[8] S. Patchkovskii, Z. Zhao, T. Brabec, and D. Villeneuve, J. Chem. Phys. **126**, 114306 (2007).
[9] S. Haessler, J. Caillat, W. Boutu, C. Giovanetti-Teixeira, T. Ruchon, T. Auguste, Z. Diveki, P. Breger, A. Maquet, B. Carré *et al.*, Nat. Phys. **6**, 200 (2010).
[10] C. Vozzi, M. Negro, F. Calegari, G. Sansone, M. Nisoli, S. De Silvestri, and S. Stagira, Nat. Phys. **7**, 823 (2011).
[11] J. L. Krause, K. J. Schafer, and K. C. Kulander, Phys. Rev. Lett. **68**, 3535 (1992).
[12] P. B. Corkum, Phys. Rev. Lett. **71**, 1994 (1993).
[13] B. K. McFarland, J. P. Farrell, P. H. Bucksbaum, and M. Gühr, Science **322**, 1232 (2008).
[14] O. Smirnova, Y. Mairesse, S. Patchkovskii, N. Dudovich, D. Villeneuve, P. Corkum, and M. Ivanov, Nature (London) **460**, 972 (2009).
[15] E. P. Fowe and A. D. Bandrauk, Phys. Rev. A **81**, 023411 (2010).
[16] A. L'Huillier and P. Balcou, Phys. Rev. Lett. **70**, 774 (1993).
[17] J. Farrell, B. McFarland, M. Gühr, and P. Bucksbaum, Chem. Phys. **366**, 15 (2009).
[18] B. K. McFarland, J. P. Farrell, P. H. Bucksbaum, and M. Gühr, Phys. Rev. A **80**, 033412 (2009).
[19] J. Higuet, H. Ruf, N. Thiré, R. Cireasa, E. Constant, E. Cormier, D. Descamps, E. Mével, S. Petit, B. Pons *et al.*, Phys. Rev. A **83**, 053401 (2011).
[20] J. B. Bertrand, H. J. Wörner, P. Hockett, D. M. Villeneuve, and P. B. Corkum, Phys. Rev. Lett. **109**, 143001 (2012).
[21] M. Lein, N. Hay, R. Velotta, J. P. Marangos, and P. L. Knight, Phys. Rev. Lett. **88**, 183903 (2002).
[22] M. Lein, N. Hay, R. Velotta, J. P. Marangos, and P. L. Knight, Phys. Rev. A **66**, 023805 (2002).
[23] T. Kanai, S. Minemoto, and H. Sakai, Nature (London) **435**, 470 (2005).
[24] C. Vozzi, F. Calegari, E. Benedetti, J.-P. Caumes, G. Sansone, S. Stagira, M. Nisoli, R. Torres, E. Heesel, N. Kajumba *et al.*, Phys. Rev. Lett. **95**, 153902 (2005).
[25] M. Lewenstein, P. Balcou, M. Y. Ivanov, A. L'Huillier, and P. B. Corkum, Phys. Rev. A **49**, 2117 (1994).
[26] D. Bauer, D. B. Milošević, and W. Becker, Phys. Rev. A **72**, 023415 (2005).
[27] O. Smirnova, M. Spanner, and M. Ivanov, J. Mod. Opt. **54**, 1019 (2007).
[28] A. Etches and L. B. Madsen, J. Phys. B **43**, 155602 (2010).
[29] X.-B. Bian and A. D. Bandrauk, Phys. Rev. A **83**, 023414 (2011).
[30] W. Hong, Q. Zhang, X. Zhu, and P. Lu, Opt. Express **19**, 26174 (2011).
[31] E. Hasović, M. Busuladžić, W. Becker, and D. B. Milošević, Phys. Rev. A **84**, 063418 (2011).
[32] S. Odžak and D. B. Milošević, J. Opt. Soc. Am. B **29**, 2147 (2012).

[33] X.-B. Bian and A. D. Bandrauk, Phys. Rev. A **86**, 053417 (2012).
[34] X. Zhu, M. Qin, Q. Zhang, Y. Li, Z. Xu, and P. Lu, Opt. Express **21**, 5255 (2013).
[35] M. D. Śpiewanowski, A. Etches, and L. B. Madsen, Phys. Rev. A **87**, 043424 (2013).
[36] S. Sukiasyan, S. Patchkovskii, O. Smirnova, T. Brabec, and M. Y. Ivanov, Phys. Rev. A **82**, 043414 (2010).
[37] Y. Okajima, O. I. Tolstikhin, and T. Morishita, Phys. Rev. A **85**, 063406 (2012).
[38] Y. Mairesse, J. Levesque, N. Dudovich, P. B. Corkum, and D. M. Villeneuve, J. Mod. Opt. **55**, 2591 (2008).
[39] G. H. Lee, I. J. Kim, S. B. Park, T. K. Kim, Y. S. Lee, and C. H. Nam, J. Phys. B **43**, 205602 (2010).
[40] H. J. Wörner, J. B. Bertrand, P. Hockett, P. B. Corkum, and D. M. Villeneuve, Phys. Rev. Lett. **104**, 233904 (2010).
[41] J. C. Baggesen and L. B. Madsen, J. Phys. B **44**, 115601 (2011).
[42] C. B. Madsen and L. B. Madsen, Phys. Rev. A **76**, 043419 (2007).
[43] C. B. Madsen, A. S. Mouritzen, T. K. Kjeldsen, and L. B. Madsen, Phys. Rev. A **76**, 035401 (2007).
[44] M. W. Schmidt, K. K. Baldridge, J. A. Boatz, S. T. Elbert, M. S. Gordon, J. H. Jensen, S. Koseki, N. Matsunaga, K. A. Nguyen, S. Su *et al.*, J. Comput. Chem. **14**, 1347 (1993).
[45] M. Born and V. Fock, Z. Phys. **51**, 165 (1928).
[46] D. Dimitrovski, C. P. J. Martiny, and L. B. Madsen, Phys. Rev. A **82**, 053404 (2010).
[47] A. Rupenyan, P. M. Kraus, J. Schneider, and H. J. Wörner, Phys. Rev. A **87**, 033409 (2013).
[48] T. H. Dunning, Jr., J. Chem. Phys. **90**, 1007 (1989).
[49] R. A. Kendall, T. H. Dunning, Jr., and R. Harrison, J. Chem. Phys. **96**, 6796 (1992).
[50] http://cccbdb.nist.gov/.
[51] H. Kono, S. Koseki, M. Shiota, and Y. Fujimura, J. Phys. Chem. A **105**, 5627 (2001).
[52] R. Torres, T. Siegel, L. Brugnera, I. Procino, J. G. Underwood, C. Altucci, R. Velotta, E. Springate, C. Froud, I. C. E. Turcu *et al.*, Phys. Rev. A **81**, 051802 (2010).
[53] A. Rupenyan, P. M. Kraus, J. Schneider, and H. J. Wörner, Phys. Rev. A **87**, 031401 (2013).
[54] X. Zhu, Q. Zhang, W. Hong, P. Lan, and P. Lu, Opt. Express **19**, 436 (2011).
[55] A. Etches, M. B. Gaarde, and L. B. Madsen, Phys. Rev. A **84**, 023418 (2011).
[56] P. Antoine, B. Piraux, and A. Maquet, Phys. Rev. A **51**, R1750 (1995).
[57] M. Peters, T. T. Nguyen-Dang, E. Charron, A. Keller, and O. Atabek, Phys. Rev. A **85**, 053417 (2012).
[58] H. Stapelfeldt and T. Seideman, Rev. Mod. Phys. **75**, 543 (2003).
[59] L. Holmegaard, J. Hansen, L. Kalhøj, S. Kragh, H. Stapelfeldt, F. Filsinger, J. Küpper, G. Meijer, D. Dimitrovski, M. Abu-Samha *et al.*, Nat. Phys. **6**, 428 (2010).
[60] M. Abu-samha and L. B. Madsen, Phys. Rev. A **82**, 043413 (2010).
[61] M. Lewenstein, P. Salières, and A. L'Huillier, Phys. Rev. A **52**, 4747 (1995).
[62] A. Wirth, M. T. Hassan, I. Grguraš, J. Gagnon, A. Moulet, T. T. Luu, S. Pabst, R. Santra, Z. A. Alahmed, A. M. Azzeer *et al.*, Science **334**, 195 (2011).
[63] O. E. Alon, V. Averbukh, and N. Moiseyev, Phys. Rev. Lett. **80**, 3743 (1998).
[64] E. Frumker, N. Kajumba, J. B. Bertrand, H. J. Wörner, C. T. Hebeisen, P. Hockett, M. Spanner, S. Patchkovskii, G. G. Paulus, D. M. Villeneuve *et al.*, Phys. Rev. Lett. **109**, 233904 (2012).
[65] P. M. Kraus, A. Rupenyan, and H. J. Wörner, Phys. Rev. Lett. **109**, 233903 (2012).